Theoretical perspective of photocatalytic properties of single-layer SnS_2

Houlong L. Zhuang and Richard G. Hennig*
Department of Materials Science and Engineering, Cornell University, Ithaca, New York 14853, USA
(Received 22 July 2013; published 30 September 2013)

We present a first-principles study of the photocatalytic properties of single-layer SnS_2. First, we calculate the formation energy and the phonon spectrum, verifying static and dynamical stability, respectively. In addition, our calculated energy of solvation suggests that single-layer SnS_2 is stable in aqueous solution. Next, by solving the Bethe-Salpeter equation, we obtain an optical band gap of 2.75 eV, consistent with the measured optical band gap. The resulting exciton binding energy of 0.41 eV is consistent with the Mott-Wannier model. Finally, by aligning the band edges with the redox potentials of water, we find that a bias potential of at least 0.9 V is required to drive the hydrogen evolution and that compressive strains can reduce this bias potential.

DOI: 10.1103/PhysRevB.88.115314 PACS number(s): 73.22.−f, 63.22.Np, 82.50.−m, 78.66.Hf

Hydrogen is regarded as the fuel of the future.[1] Generating hydrogen from solar water splitting via a semiconducting photocatalyst is a promising clean solution to overcome the existing energy shortage problems.[2] In addition to their attractive electronic properties,[3–5] single-layer materials have recently been shown by both theoretical calculations and experiments to function as potential photocatalysts for water splitting. For example, theoretical studies have predicted that single-layer transition metal dichalcogenides and group-III monochalcogenides are potential photocatalysts for water splitting.[6–9]

Experiments show evidence that several single-layer materials are advantageous over their three-dimensional (3D) counterparts for use as photocatalysts. One representative example is the study by Sun *et al*. for single-layer SnS_2 as a photocatalyst for solar water splitting.[10] The work shows that the incident photon-to-current conversion efficiency of single-layer SnS_2 can approach 38.7%, in striking contrast to the low efficiency of 2.33% of 3D bulk SnS_2. Single-layer SnS_2 exhibits a hexagonal structure with space group $P\bar{3}m1$. Figure 1 shows that the single-layer structure consists of three atomic sublayers, with Sn atoms forming the center sublayer bonded to six nearest-neighbor S atoms located in the top and bottom sublayers.

In this work we determine the stability, band gap, and band-edge positions of single-layer SnS_2, which are of importance for the material being a potential photocatalyst. We show that single-layer SnS_2 exhibits a low formation energy, dynamically stable phonon modes, and a high energy of solvation. Furthermore, we determine the optical band gap of single-layer SnS_2 as 2.75 eV, right within the range of visible light. Moreover, we show that the lowest-energy exciton in single-layer SnS_2 is accurately described by the Mott-Wannier model.[11] Finally, we show that an external bias potential of at least 0.9 V is required to drive the hydrogen evolution and that compressive strains can reduce this bias potential.

We perform density functional theory (DFT) calculations using the projector-augmented wave method as implemented in the plane-wave code VASP.[12–14] For the structural relaxations we employ both the Perdew-Burke-Ernzerhof (PBE) generalized gradient approximation and the Heyd-Scuseria-Ernzerhof (HSE06) hybrid functional.[15,16] For the phonon calculations, we use a cutoff energy of 600 eV to ensure the convergence, particularly of the low-energy phonon modes. For all other calculations, a cutoff energy of 400 eV ensures an energy accuracy of 1 meV/atom. The k-point sampling uses the Monkhorst-Pack scheme[17] and employs for the single-layer materials a $48 \times 48 \times 1$ mesh for the PBE functional and an $18 \times 18 \times 1$ mesh for the more expensive HSE06, G_0W_0, and Bethe-Salpeter calculations. For the single-layer SnS_2 calculations, a vacuum spacing of 18 Å ensures that the interactions between the layers are negligible.

The electron-hole interaction plays an important role in the optical response of a material.[18] We calculate the optical spectra of single-layer SnS_2, including the excitonic interaction, by solving the Bethe-Salpeter equation (BSE) implemented in the VASP code.[19,20] The BSE spectrum calculations start with the G_0W_0 quasiparticle energies and the PBE wave functions. The G_0W_0 calculations use 192 bands and 128 frequency points. The 12 highest valence and 16 lowest conduction bands are included in the calculation of the excitonic states.

To determine the stability of single-layer SnS_2 in aqueous solution we use GAUSSIAN09 (Refs. 21 and 22) to calculate the hydration energy using the PBE functional. We employ the aug-cc-pVQZ basis sets, and for the heavy atom Sn we use effective core potentials.[23,24] The energy of the solvated ions is calculated using several explicit water molecules and the density-based solvation model (SMD) for the solute-solvent interactions.[22] We find that three water molecules are required to converge the hydration energy to 4 kJ/mol.

To be a useful material, single-layer SnS_2 needs to be stable, particularly in an aqueous environment. We determine the stability of single-layer SnS_2 by calculating its formation energy relative to the 3D bulk phase, its dynamic stability, and its solvation energy in water.

We first determine the structural parameters of single-layer SnS_2. Table I shows that bulk- and single-layer SnS_2 exhibit similar structural parameters and elastic moduli. The generalized gradient approximation slightly overestimates the in-plane lattice parameter of bulk SnS_2 compared to the experimental value of 3.65 Å.[25] The HSE06 lattice parameter of single-layer SnS_2 is smaller than the PBE counterpart, since HSE06 includes 25% of exact exchange, reducing the self-interaction error in the PBE functional and improving the agreement with experimental lattice parameters.[26] The

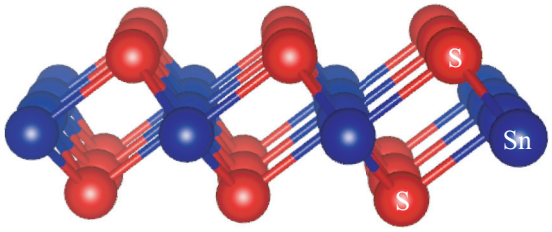

FIG. 1. (Color online) Crystal structure of single-layer SnS_2. Each sulfur atom (red ball) has three neighboring tin atoms, while each tin atom (blue ball) has six neighboring sulfur atoms.

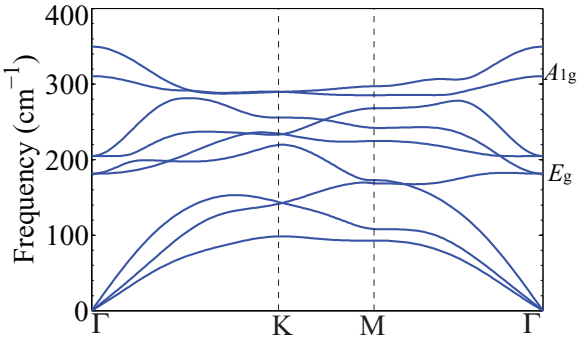

FIG. 2. (Color online) Phonon spectrum of single-layer SnS_2. The Raman-active modes at Γ are denoted as A_{1g} and E_g, respectively.

elastic modulus of single-layer SnS_2 is significantly smaller than that of MoS_2, which exhibits an experimental mean value of 180 N/m.[27]

To test the stability of single-layer SnS_2 relative to the energy of bulk SnS_2, we calculate its formation energy E_f as $E_f = E_{2D} - E_{3D}$. To accurately account for dispersion interactions, we use the vdw-optB88 van der Waals functional for the calculation of the formation energy. This functional accurately describes lattice constants and cohesive energies.[28] Without van der Waals interactions the single-layer SnS_2 incorrectly becomes the ground state. The resulting formation energy of single-layer SnS_2 is only 80 meV/atom higher than that of the bulk phase. This low formation energy is comparable to that of single-layer transition metal dichalcogenides such as MoS_2 and other group-III monochalcogenides such as GaS and GaSe, all of which have been successfully synthesized by micromechanical exfoliation.[8,9,29]

To determine the dynamical stability of single-layer SnS_2, we obtain its phonon spectrum from the force constants calculated with density functional perturbation theory[30,31] and the PBE functional. Figure 2 shows the phonon spectrum of single-layer SnS_2. No imaginary frequencies are observed, confirming the dynamical stability of single-layer SnS_2. The irreducible representation of the phonon modes at the center of the Brillouin zone is given by $\Gamma = A_{1g} + 2A_{2u} + E_g + 2E_u$.[32] Two of these six modes, the A_{1g} and E_g modes denoted in Fig. 2, are Raman active.[31] Our calculated phonon frequencies for the A_{1g} and E_g modes are 311 and 181 cm^{-1}, respectively. This is in excellent agreement with the experimental values of 310 and 200 cm^{-1}, respectively,[10] indicating the accuracy of DFT for single-layer SnS_2.

We then assess the stability of single-layer SnS_2 in water by calculating the solvation energy when crystalline SnS_2 is decomposed into Sn and S ions in aqueous solution. We first obtain the cohesive energy from the PBE functional as implemented in VASP and then calculate the hydration energy using the GAUSSIAN09 package.[21] The solvation energy is given by the sum of these two energies.[8,9] This method has been successfully applied to determine the stability of other single-layer materials such as MoS_2 and group-III monochalcogenides.[8,9] The resulting solvation energy of single-layer SnS_2 is 620 kJ/mol, significantly larger than that of other poorly soluble compounds such as CuS, exhibiting solvation energies ranging from 300 to 400 kJ/mol.[33] Taking into account ion association where a solvated cation-anion pair is formed, we obtain an almost identical solvation energy of 619 kJ/mol. The high solvation energy implies the stability of single-layer SnS_2 in aqueous solution.

Figure 3 shows the band structures of single-layer SnS_2 obtained from the PBE and HSE06 functionals and the G_0W_0 method. SnS_2 displays an indirect band gap with the valence band maximum (VBM) located between the Γ and M points, while the conduction band minimum (CBM) occurs at the M point. Table II compares the direct and indirect fundamental band gaps of single-layer SnS_2 from these three different approaches with the experimental optical band gaps.[34] The PBE functional as usual underestimates the band gaps[35] and predicts gaps 1 eV smaller than the HSE06 functional and the G_0W_0 approximation. The HSE06 and G_0W_0 methods

TABLE I. Structural parameters and elastic modulus of single-layer and bulk SnS_2. The parameters include the lattice parameter a_0, the Sn-S bond length $b_{Sn\text{-}S}$, S-S bond length $b_{S\text{-}S}$ in units of Å, and the Sn-S-Sn bond angle $\theta_{Sn\text{-}S\text{-}Sn}$ in units of degrees. The elastic modulus C is in units of N/m.

System	Functional	a_0	$b_{Sn\text{-}S}$	$b_{S\text{-}S}$	$\theta_{Sn\text{-}S\text{-}Sn}$	C
Single layer	PBE	3.70	2.60	3.65	90.75	87
	vdw-optB88	3.69	2.60	3.66	90.58	90
	HSE06	3.64	2.56	3.59	90.80	102
Bulk	vdw-optB88	3.71	2.60	3.66	90.82	89

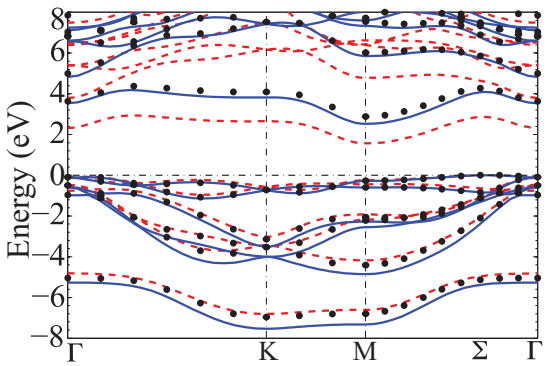

FIG. 3. (Color online) Band structure of single-layer SnS_2 calculated with the PBE (red dashed line) and HSE06 (blue solid line) functionals and the G_0W_0 method (black dots).

TABLE II. Fundamental indirect and direct band gaps (in eV) of single-layer SnS_2 obtained from three different approaches. Experimental optical band gaps are shown for comparison.[34]

Gap	E_g^{PBE}	E_g^{HSE06}	$E_g^{G_0W_0}$	Experiment
Indirect (Σ-M)	1.57	2.52	2.88	2.23
Direct (M-M)	1.81	2.81	3.16	2.55

predict similar band gaps, with the G_0W_0 band gaps being about 0.35 eV larger. However, all three methods show that the difference between the indirect and direct band gaps is small, with a value of 0.3 eV, consistent with the difference of the experimental optical band gaps.[34] Furthermore, the band gaps of single-layer SnS_2 are well positioned within the range of 1.7–3.0 eV that is required for efficient photocatalytic water splitting.[36,37]

To understand the bonding characteristics of single-layer SnS_2, we analyze the total and projected density of states (TDOS and PDOS) within the energy window of −4 to 4 eV with reference to the VBM. Figure 4 shows that the TDOS at the valence band edge is as large as 2.8 states/(eV unit cell). Such a large DOS is suggested as a main contributing factor to the prominent visible-light conversion efficiency of single-layer SnS_2.[10] The corresponding PDOS of SnS_2 in Fig. 4 illustrates that the valence band of SnS_2 from −2 to 0 eV is dominated by the S $3p$ states, whereas in the lower energy window between −4 and −2 eV, it mainly consists of hybridized states of S $3p$ and Sn $5p$ orbitals.

Figure 5 shows the imaginary part of the permittivity ϵ_2 calculated from the Bethe-Salpeter equation and random-phase approximation (RPA), respectively. Similar to single-layer MoS_2, the BSE optical absorption spectrum is dominated by resonant excitonic states.[38,39] Three absorption peaks are observed in the low-energy region below 3.2 eV of the BSE spectrum. In contrast, no peaks are observed in the RPA spectrum of the same energy window, indicating the importance of considering excitonic effects. The first peak, located at an energy of 2.75 eV, corresponds to the direct optical band gap at the M point. This energy agrees well with the experimental direct optical band gap of 2.55 eV measured by UV-visible transmission spectroscopy.[34] The second peak appears at 2.92 eV due to another exciton, and the third peak corresponds to the direct quasiparticle band gap of 3.16 eV obtained with the G_0W_0

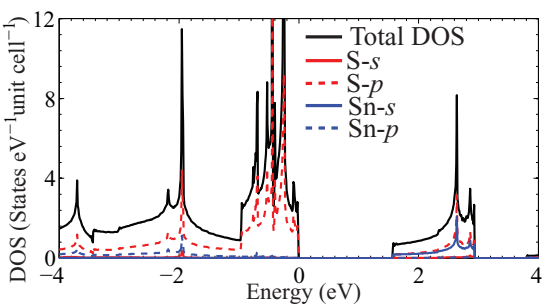

FIG. 4. (Color online) Total and projected density of states of single-layer SnS_2.

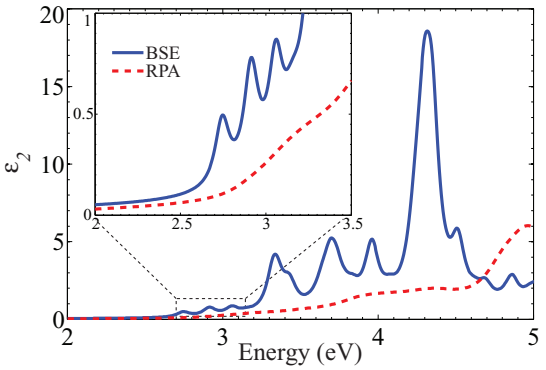

FIG. 5. (Color online) Imaginary part of the permittivity calculated with the BSE and RPA scheme. The inset shows a closeup of the first three BSE peaks. To compensate for the band-gap underestimation using the PBE functional in the RPA calculation, we shift the spectra by 1.0 eV, which is the difference between the HSE06 and PBE band gaps.

method. The energy difference between the first and third peak gives an exciton binding energy of 0.41 eV, close to the value of 0.4 eV for bulk SnS_2,[40] and also comparable to the exciton binding energy of single-layer MoS_2 and WS_2 of 0.6 eV.[39]

The Mott-Wannier model has recently been applied to estimate the exciton binding energy of single-layer MoS_2.[11,41] It is worthwhile testing whether this model is applicable to the excitons in single-layer SnS_2 as well. In this model excitons form hydrogen-like states. In two dimensions, the first excitonic binding energy is

$$E_0 = 4\frac{m_r}{m_0}\frac{R_\infty}{\epsilon_{2D}^2}, \tag{1}$$

where m_r is the reduced effective electron mass, m_0 the rest mass of the electron, ϵ_{2D} the effective permittivity, and R_∞ the Rydberg constant.[41]

For 2D systems, subtleties arise since the calculated permittivity tensor depends on the size of the simulation cell, i.e., the thickness of the vacuum layer. To determine the permittivity of single-layer SnS_2, ϵ_{SnS_2}, we treat each cell as a composite of one layer of SnS_2 and one layer of vacuum with $\epsilon_{vac} = 1$. We approximate the thickness of single-layer SnS_2 as 5.89 Å, which is the interlayer distance in bulk SnS_2 calculated with the vdw-optB88 van der Waals functional. Using the linear law,[42] $\epsilon_{calc} = f \cdot \epsilon_{SnS_2} + (1 - f) \cdot \epsilon_{vac}$, where f is the volume fraction of the SnS_2 layer in a simulation cell, we fit the permittivity of single-layer SnS_2 from the calculated permittivity ϵ_{calc} for cells of dimension 10, 18, and 25 Å. This results in the relative permittivity parallel to the sheet of $\epsilon_\parallel = 8.17$, perpendicular to it of $\epsilon_\perp = 2.41$, and the effective permittivity of $\epsilon_{2D} = \sqrt{\epsilon_\parallel \cdot \epsilon_\perp}$. We obtain the reduced effective electron mass from $1/m_r = 1/m_e + 1/m_h$, where $m_e = 0.25\,m_0$ and $m_h = 0.37\,m_0$ are the electron and hole effective masses, respectively, at the M point obtained from the HSE06 band structure. The exciton binding energy predicted from the Mott-Wannier model is 0.41 eV, identical to the binding energy calculated by solving the Bethe-Salpeter equation. While such perfect agreement is probably somewhat

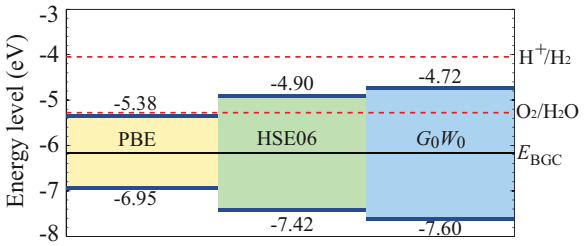

FIG. 6. (Color online) Energy diagram of single-layer SnS_2 with respect to normal hydrogen electrode levels in electrolyte of pH = 6.6. The CBM and VBM energy levels are obtained from the HSE06 band-gap center in combination with the band gaps from three different approaches, including the PBE functional (1.57 eV), the HSE06 functional (2.52 eV), and the G_0W_0 method (2.88 eV).

fortuitous, it nevertheless indicates that the exciton in single-layer SnS_2 is a Mott-Wannier–type exciton.

To determine under what conditions single-layer SnS_2 is able to photocatalytically split water, we calculate the band-edge positions E_{CBM} and E_{VBM} relative to the vacuum level and compare them with the reduction and oxidation potentials of water. We follow the method by Toroker *et al.*[43] and determine the CBM and VBM levels from the band-gap center energy E_{BGC} relative to the vacuum level and the value of the band gap E_g:

$$E_{CBM/VBM} = E_{BGC} \pm \tfrac{1}{2} E_g. \quad (2)$$

This method takes advantage of the observation that the band-gap center energy is relatively insensitive to the exchange-correlation functional used.[9,43] The approach also allows for the combination of different methods for the band-gap center energy and the band gap. The energy difference between the band-gap center and the vacuum level is obtained as the average electrostatic potential halfway in between the SnS_2 layers. For the HSE06 functional we obtain $E_{BGC} = -6.16$ eV relative to the vacuum level, and for the PBE functional $E_{BGC} = -6.04$ eV. Similar to our previous study on group-III monochalcogenides,[9] we observe that the band-gap center energy depends only weakly on the functional.

In a number of studies of various materials, including single-layer MoS_2 and bulk Ag_3PO_4, the band-gap center energy is determined from the Mulliken electronegativity χ.[6,44,45] We test this phenomenological model for single-layer SnS_2 and calculate the Mulliken electronegativity χ of single-layer SnS_2 as the geometric mean $\chi = (\chi_{Sn}^m \chi_S^n)^{1/(m+n)}$ of the electronegativities of Sn and S atoms, χ_{Sn} and χ_S, respectively, with $m = 1$ and $n = 2$ for SnS_2.[46] The Mulliken electronegativity of an atom is given by the average of the electron affinity and first ionization potential. Using experimental data for the electron affinity and ionization potential,[33] we obtain a χ for SnS_2 of -5.47 eV. This empirical value significantly overestimates the band-gap center energy, indicating that the empirical model does not accurately predict the band-edge positions of single-layer SnS_2.

Figure 6 shows the band-edge positions of the CBM and the VBM obtained from Eq. (2) using the HSE06 band-gap center energy with the PBE and HSE06 fundamental gaps and the G_0W_0 quasiparticle gap. To determine the bias potential at which SnS_2 is able to photocatalytically split water, we compare the calculated band-edge positions with the reduction and oxidation potentials of water. These potentials depend on the pH value, i.e., the standard reduction potential for H^+/H_2 is $E^{red}_{H^+/H_2} = -4.44\,\text{eV} + \text{pH} \times 0.059\,\text{eV}$.[47] In the experimental study of Ref. 10, the use of 0.5 M Na_2SO_4 electrolyte resulted in a pH value of 6.6. Using this value we obtain for the reduction potential $E^{red}_{H^+/H_2} = -4.05$ eV and for the oxidation potential $E^{ox}_{O_2/H_2O} = -5.28$ eV.

The comparison of the water reduction and oxidation potentials with the band-edge positions of single-layer SnS_2 in Fig. 6 shows that although the VBM is energetically favorable for oxygen evolution, the CBM is insufficient to drive the hydrogen evolution. Therefore an external bias potential is needed for photocatalytic water splitting. Such bias potentials decrease the efficiency for water splitting.[2] We find that a minimum bias potential of 0.9 V is required to shift the HSE06 CBM above the reduction potential of H^+/H_2. An additional overpotential of the order of a few tenths of electronvolts is required to overcome various activation barriers, with the overpotential for the hydrogen evolution reaction being typically smaller than the one for the oxygen evolution reaction.[48] Comparing the calculated minimum bias potential of 0.9 eV with the reported experimental bias potential of 1.0 eV (Ref. 10) indicates a small overpotential for the hydrogen evolution for single-layer SnS_2, on the order of a tenth of an electronvolt.

Strain engineering can be used to reduce the bias potential. Using the HSE06 functional, we predict that compressive strains are favorable. A 4% biaxial compressive strain decreases the band gap to 2.38 eV and increases the CBM and VBM band edges to -4.65 and -7.03 eV, respectively. This reduces the required bias potential for hydrogen evolution from 0.9 to 0.6 V and improves the efficiency for photocatalytic water splitting.

In summary, we have investigated several important aspects of using single-layer SnS_2 as a photocatalyst for water splitting. We show that single-layer SnS_2 has a low formation energy relative to bulk SnS_2, is dynamically stable, and stable in aqueous solution. By solving the Bethe-Salpeter equation, we obtain an optical band gap of 2.75 eV and an exciton binding energy of 0.41 eV. The optical band gap lies within the range of visible light, implying that a significant fraction of solar light can be harvested by single-layer SnS_2. Finally, we show that a bias potential of at least 0.9 V is needed for the water splitting to proceed and that compressive strains can reduce the required bias potential. Overall, our simulation results support the experimental finding that single-layer SnS_2 is a promising photocatalyst for water splitting.[10]

We thank M. Spencer, D. Muller, F. Rana, and D. Schlom for helpful discussions. This work was supported by the NSF through the Cornell Center for Materials Research under Award No. DMR-1120296 and by the NSF CAREER Award No. DMR-1056587. This research used computational resources of the Texas Advanced Computing Center under Contract No. TG-DMR050028N and of the Computation Center for Nanotechnology Innovation at Rensselaer Polytechnic Institute.

*rhennig@cornell.edu

[1] T. Bak, J. Nowotny, M. Rekas, and C. Sorrell, Int. J. Hydrogen Energy **27**, 991 (2002).

[2] M. G. Walter, E. L. Warren, J. R. McKone, S. W. Boettcher, Q. Mi, E. A. Santori, and N. S. Lewis, Chem. Rev. **110**, 6446 (2010).

[3] K. F. Mak, C. Lee, J. Hone, J. Shan, and T. F. Heinz, Phys. Rev. Lett. **105**, 136805 (2010).

[4] B. Radisavljevic, A. Radenovic, B. J. V. Giacometti, and A. Kis, Nat. Nanotechnol. **6**, 147 (2011).

[5] Q. H. Wang, K. Kalantar-Zadeh, A. Kis, J. N. Coleman, and M. S. Strano, Nat. Nanotechnol. **7**, 699 (2012).

[6] N. Singh, G. Jabbour, and U. Schwingenschlögl, Eur. Phys. J. B **85**, 392 (2012).

[7] J. Kang, S. Tongay, J. Zhou, J. Li, and J. Wu, Appl. Phys. Lett. **102**, 012111 (2013).

[8] H. L. Zhuang and R. G. Hennig, J. Phys. Chem. C (2013), doi: 10.1021/jp405808a.

[9] H. L. Zhuang and R. G. Hennig, Chem. Mater. **25**, 3232 (2013).

[10] Y. Sun, H. Cheng, S. Gao, Z. Sun, Q. Liu, Q. Liu, F. Lei, T. Yao, J. He, S. Wei, and Y. Xie, Angew. Chem. Int. Ed. **51**, 8727 (2012).

[11] J. M. Ziman, *Principles of the Theory of Solids* (Cambridge University Press, Cambridge, UK, 1979).

[12] G. Kresse and J. Furthmüller, Phys. Rev. B **54**, 11169 (1996).

[13] P. E. Blöchl, Phys. Rev. B **50**, 17953 (1994).

[14] G. Kresse and D. Joubert, Phys. Rev. B **59**, 1758 (1999).

[15] J. P. Perdew, K. Burke, and M. Ernzerhof, Phys. Rev. Lett. **77**, 3865 (1996).

[16] J. Heyd, G. E. Scuseria, and M. Ernzerhof, J. Chem. Phys. **118**, 8207 (2003).

[17] H. J. Monkhorst and J. D. Pack, Phys. Rev. B **13**, 5188 (1976).

[18] G. Onida, L. Reining, and A. Rubio, Rev. Mod. Phys. **74**, 601 (2002).

[19] C. Rödl and F. Bechstedt, Phys. Rev. B **86**, 235122 (2012).

[20] P. Rinke, A. Schleife, E. Kioupakis, A. Janotti, C. Rödl, F. Bechstedt, M. Scheffler, and C. G. Van de Walle, Phys. Rev. Lett. **108**, 126404 (2012).

[21] M. J. Frisch, G. W. Trucks, H. B. Schlegel, G. E. Scuseria, M. A. Robb, J. R. Cheeseman, G. Scalmani, V. Barone, B. Mennucci, G. A. Petersson *et al.*, *Gaussian 09, Revision D.01* (Gaussian Inc., Wallingford, CT, 2009).

[22] A. V. Marenich, C. J. Cramer, and D. G. Truhlar, J. Phys. Chem. B **113**, 6378 (2009).

[23] K. L. Schuchardt, B. T. Didier, T. Elsethagen, L. Sun, V. Gurumoorthi, J. Chase, J. Li, and T. L. Windus, J. Chem. Inf. Model. **47**, 1045 (2007).

[24] D. Feller, J. Comput. Chem. **17**, 1571 (1996).

[25] F. Al-Alamy, A. Balchin, and M. White, J. Mater. Sci. **12**, 2037 (1977).

[26] R. G. Hennig, A. Wadehra, K. P. Driver, W. D. Parker, C. J. Umrigar, and J. W. Wilkins, Phys. Rev. B **82**, 014101 (2010).

[27] S. Bertolazzi, J. Brivio, and A. Kis, ACS Nano **5**, 9703 (2011).

[28] J. Klimeš, D. R. Bowler, and A. Michaelides, Phys. Rev. B **83**, 195131 (2011).

[29] K. S. Novoselov, D. Jiang, F. Schedin, T. J. Booth, V. V. Khotkevich, S. V. Morozov, and A. K. Geim, Proc. Nat. Acad. Sci. USA **102**, 10451 (2005).

[30] S. Baroni, S. de Gironcoli, A. Dal Corso, and P. Giannozzi, Rev. Mod. Phys. **73**, 515 (2001).

[31] M. Gajdoš, K. Hummer, G. Kresse, J. Furthmüller, and F. Bechstedt, Phys. Rev. B **73**, 045112 (2006).

[32] A. J. Smith, P. E. Meek, and W. Y. Liang, J. Phys. C **10**, 1321 (1977).

[33] *CRC Handbook of Chemistry and Physics*, 93rd ed., edited by D. P. Lide (CRC Press, Boca Raton, FL, 2012).

[34] H. Zhong, G. Yang, H. Song, Q. Liao, H. Cui, P. Shen, and C.-X. Wang, J. Phys. Chem. C **116**, 9319 (2012).

[35] J. P. Perdew, Int. J. Quant. Chem. **30**, 451 (1986).

[36] R. van de Krol and M. Grätzel, *Photoelectrochemical Hydrogen Production* (Springer, New York, 2011).

[37] A. Kudo and Y. Miseki, Chem. Soc. Rev. **38**, 253 (2009).

[38] J. Feng, X. Qian, C.-W. Huang, and J. Li, Nat. Photon. **6**, 866 (2012).

[39] H. Shi, H. Pan, Y.-W. Zhang, and B. I. Yakobson, Phys. Rev. B **87**, 155304 (2013).

[40] Y. Bertrand, G. Leveque, J. Robin, and R. Mamy, Physica B+C **99**, 287 (1980).

[41] T. Cheiwchanchamnangij and W. R. L. Lambrecht, Phys. Rev. B **85**, 205302 (2012).

[42] A. Sihvola, *Electromagnetic Mixing Formulae and Applications* (The Institution of Engineering and Technology, London, 2000).

[43] M. C. Toroker, D. K. Kanan, N. Alidoust, L. Y. Isseroff, P. Liao, and E. A. Carter, Phys. Chem. Chem. Phys. **13**, 16644 (2011).

[44] H. Jiang, J. Phys. Chem. C **116**, 7664 (2012).

[45] J. J. Liu, X. L. Fu, S. F. Chen, and Y. F. Zhu, Appl. Phys. Lett. **99**, 191903 (2011).

[46] A. H. Nethercot, Phys. Rev. Lett. **33**, 1088 (1974).

[47] V. Chakrapani, J. C. Angus, A. B. Anderson, S. D. Wolter, B. R. Stoner, and G. U. Sumanasekera, Science **318**, 1424 (2007).

[48] S. S. Kocha and J. A. Turner, J. Electrochem. Soc. **142**, 2625 (1995).